Numerical simulations of aggregate breakup in bounded and unbounded turbulent flows

Numerical simulations of aggregate breakup in bounded and unbounded turbulent flows

Matthaus U. Babler,[1,*] Luca Biferale,[2] Luca Brandt,[3] Ulrike Feudel,[4] Ksenia Guseva,[4] Alessandra S. Lanotte,[5] Cristian Marchioli,[6] Francesco Picano,[3] Gaetano Sardina,[3] Alfredo Soldati,[7] and Federico Toschi[8]

[1]*Department of Chemical Engineering and Technology, KTH Royal Institute of Technology, SE-10044 Stockholm, Sweden*
[2]*Dept. of Physics and INFN, University of Rome Tor Vergata, Via della Ricerca Scientifica 1, 00133 Roma, Italy*
[3]*Linné FLOW Center and SeRC (Swedish e-Science Research Centre), KTH Mechanics, SE-10044 Stockholm, Sweden*
[4]*Theoretical Physics/Complex Systems, ICBM, Carl von Ossietzky University, Oldenburg, Germany*
[5]*ISAC-CNR, Str. Prov. Lecce-Monteroni, and INFN, Sez. Lecce, 73100 Lecce, Italy*
[6]*Dept. of Electrical, Managerial and Mechanical Engineering, University of Udine, Udine, Italy, and Dept. Fluid Mechanics, CISM, Udine, Italy*
[7]*Dept. of Electrical, Managerial and Mechanical Engineering, University of Udine, 33100 Udine, Italy, and Dept. Fluid Mechanics, CISM, 33100 Udine, Italy*
[8]*Dept. Applied Physics, Eindhoven University of Technology, 5600 MB Eindhoven, the Netherlands and IAC, CNR, Via dei Taurini 19, 00185 Roma, Italy*

(Dated: June 12, 2014)

Breakup of small aggregates in fully developed turbulence is studied by means of direct numerical simulations in a series of typical bounded and unbounded flow configurations, such as a turbulent channel flow, a developing boundary layer, and homogeneous isotropic turbulence. Aggregate breakup occurs when the local hydrodynamic stress $\sigma \sim \varepsilon^{1/2}$, where ε is the energy dissipation at the position of the aggregate, overcomes a given threshold $\sigma_{\rm cr}$, characteristic for a given type of aggregates. Results show that the breakup rate decreases with increasing threshold. For small thresholds, it develops a universal scaling among the different flows. For high thresholds, the breakup rates show strong differences among the different flow configurations, highlighting the importance of non-universal mean-flow properties. To further assess the effects of flow inhomogeneity and turbulent fluctuations, results are compared with those obtained in a smooth stochastic flow. Furthermore, we discuss limitations and applicability of a set of independent proxies.

INTRODUCTION

Particles in the colloidal and micrometer size range have a strong tendency to stick together and form aggregates that, depending on the type of particles and the environment, might undergo further transformations such as coalescence or sintering to form compact structures. Turbulence in the suspending fluid has a distinct influence on the aggregation process: It leads to an enhancement of the rate at which aggregates grow, i.e. by facilitating collisions among particles [1, 2, 3, 4], and it induces breakup of the formed aggregates [5, 6, 7, 8]. Breakup is an important phenomenon in aggregation processes [9, 10, 11], as it is one of the two main mechanisms that can interrupt aggregate growth in a destabilized suspension of infinite extent (the other mechanism is sedimentation which removes large aggregates from the suspension). This is experimentally evidenced by monitoring the evolution of the aggregate size in a stirred suspension of destabilized particles [12, 13]. Starting from primary particles, the aggregate size first undergoes a rapid increase before leveling off to a plateau, where aggregation and breakup balance each other. Increasing at this point the stirring increases the magnitude of breakup which results in a rapid relaxation of the aggregate size to a new plateau at a lower size.

Breakup of aggregates has attracted considerable attention in the literature [14, 15, 16, 17]. The aggregate strength is experimentally measured by immersing pre-prepared aggregates into a sufficiently diluted flow and measuring the size and structure of the fragments that do not undergo further breakup [6, 18, 19, 20]. Assuming that the largest fragments are the remainder of the original clusters, it allows for interpreting the measured fragment size as the aggregate strength. From such experiments it was found that the typical aggregate size that can withstand breakup decreases as a power law with the applied hydrodynamic stress, or put the other way around, the aggregate strength decreases with increasing the size. However, the strength *per se* gives no information on the rate of breakup, i.e. how fast the number of aggregates decays in time. The rate of breakup is a crucial quantity regarding the dynamics of aggregation processes since it influences restructuring [21] and crucially controls the steady state cluster size distribution [22]. Moreover, it is an important quantity for modeling aggregation processes by means of population balance equations, where breakup typically is described as a rate process [5, 23, 24].

Early models relating the breakup rate to the aggregate strength were presented by Delichatsios [25] and Loginov [26] (for the conceptual equivalent case of

breakup of sub-Kolmogorov droplets), followed by the exponential model of Kusters [27] and the engulfment model of Babler et al. [28]. The basic principle is that an aggregate suspended in a turbulent flow is subject to a fluctuating hydrodynamic stress that only intermittently overcomes the critical stress required to break the aggregate. The breakup rate is then derived from the time it takes for an aggregate to experience such stress.

Describing how long it takes for an aggregate to experience a breaking stress is not an easy task, as the fluctuations in the stress experienced by an aggregate are not only controlled by turbulent fluctuations but also by the way the moving aggregate samples these fluctuations. Accordingly, predicted breakup rates vary strongly among the different models and even lead to contradictory results: in the limit of very weak aggregates the exponential model of Kusters [27] predicts a constant breakup rate, while the engulfment model leads to a diverging breakup rate [28]. In Babler et al. [29], direct numerical simulations (DNS) were used to obtain Lagrangian trajectories of point-like aggregates released into homogeneous and isotropic turbulence (HIT): trajectories were followed until the aggregates experienced a stress that is able to break them. The breakup rate measured in this study showed some characteristic properties that were only partially captured by earlier models. In particular, for small values of the aggregate strength, the breakup rate follows a power law, while in the opposite limit of the aggregate strength becoming large, the breakup rate decreases with a sharp super-exponential cut off. While the behavior at large aggregate strength was well captured by the engulfment model, the power law behavior was overestimated by both the engulfment and exponential model. More recently, a similar analysis [30] was performed by combining data obtained from a DNS of HIT with discrete element methods based on Stokesian dynamics, that models in detail the internal stresses while the aggregates are moving in the turbulent field. This more detailed analysis confirmed the power law behavior of the breakup rate in the limit of small aggregate strength, while in the opposite limit of large strength, a slightly slower drop off was observed, due to the role of internal stresses and aggregate orientation in the flow.

Most of the works presented so far considered aggregate dynamics in homogeneous and isotropic turbulence, which for real turbulent flows only holds on a sufficiently small length-scale and for distances far enough from the walls. The question thus arises to which extent results from homogeneous flows apply to real flows, which are strongly influenced by their boundary conditions. To this aim, in this work we investigate breakup of aggregates in wall-bounded flows, namely a developing boundary layer flow and a channel flow. Aggregate breakup is studied by means of numerical experiments using the same methodology as in our previous work [29]. Specifically, the aggregates are assumed small with respect to the viscous length scale of the flow, and their inertia is negligible. Furthermore, their concentration is assumed low such that the properties of the flow are not altered due to the presence of the aggregates. Breakup is assumed to occur whenever the hydrodynamic stress, taken as the local energy dissipation at the position of the aggregate, exceeds a predefined threshold representing the aggregate strength. In future works, this assumption might be refined by introducing some internal dynamics leading to stretching-relaxation dynamics similar as for the case of droplet deformation/breakup and the polymer coil/stretch transition in turbulent flows [31, 32, 33].

For both flows, we consider the situations where aggregates are released close to the wall and far away from it. Despite the strong non-homogeneity and the presence of a mean shear in wall-bounded flows, the measured breakup rate in each of these cases shows some remarkable similarities to the breakup rate in homogeneous turbulence. To corroborate and better understand this behavior, we additionally consider a synthetic turbulent flow obtained by stochastically evolving the Fourier modes of a random velocity field. Measuring the breakup rate in this flow leads to similar power law behavior suggesting that the latter is caused by weak turbulent fluctuations, well represented by Gaussian statistics and therefore only weakly influenced by the flow's boundary condition. The breakup rate of strong aggregates, on the other hand, is substantially larger in wall-bounded flows, when compared with homogeneous turbulence where only rare intermittent burst can break strong aggregates.

NUMERICAL EXPERIMENTS

Aggregate breakup in turbulent flows

As in Babler et al. [29], we consider a situation where preformed aggregates are released at a given location into a stationary flow containing otherwise no particles. The flow is assumed to be diluted such that its statistical properties are not affected by the presence of the aggregates (one-way coupling between the fluid and the particulate phase). Furthermore, the aggregate density is assumed to be close to the fluid density, and their size is small with respect to the dissipative length scale of the flow but large enough for Brownian motion to be negligible. The aggregate Stokes time $\tau_p = (2\rho_p + \rho)r^2/(9\rho\nu)$ where ρ is the fluid density, ρ_p is the aggregate density, ν is the kinematic viscosity, and r is the aggregate radius, is thus small with respect to the fastest turbulent timescale. On the one hand, this implies that the aggregates have negligible inertia and their motion can be treated as if they were tracers. On the other hand, it identifies the breakup mechanism to be due to hydrodynamic stress acting on the aggregate.

We define breakup as a singular event in time, i.e. there is an exact moment in time when an aggregate turns from being intact into being broken. We assume that this happens when the local stress acting on the aggregate exceeds a critical stress $\sigma_{\rm cr}$ [28, 29]. The latter is a characteristic of the considered aggregate, i.e. $\sigma_{\rm cr}$ is a function of the aggregate properties such as size, structure, type of the constituting particles, and chemical environment. Among these variables, the size of the aggregate is most crucial. A large body of experimental [18, 19, 20], numerical [17, 34, 35, 36], and theoretical studies [14] suggest a power law dependency of the form

$$\sigma_{\rm cr} \sim r^{-q}, \quad \text{respectively} \quad \sigma_{\rm cr} \sim \xi^{-q/d_f}, \qquad (1)$$

where $\xi \sim r^{d_f}$ is the number of primary particles constituting the aggregate, d_f is the aggregate fractal dimension, and q is a scaling exponent that depends on the aggregate structure. For dense but non-compact aggregates, Zaccone et al. [14] give $q = [9.2(3 - d_f) + 1]/2$ in good agreement with experiments [20, 37].

The hydrodynamic stress acting on an aggregate is $\sigma \sim \mu(\varepsilon/\nu)^{1/2}$, where μ is the dynamic viscosity and ε is the local energy dissipation rate defined as:

$$\varepsilon = 2\nu s_{ij} s_{ij}\,, \qquad (2)$$

where $s_{ij} = \frac{1}{2}(\partial u_i/\partial x_j + \partial u_j/\partial x_i)$. Thus, strong fluctuations of ε control the fluctuations of the stress and therefore the occurrence of breakup events. This translates into a picture where an aggregate upon release moves through the flow until the local dissipation exceeds a threshold value $\varepsilon_{\rm cr} \sim [\sigma_{\rm cr}(\xi)]^2$ causing it to break up. Hence, it is crucial to control the typical time the aggregate experiences a local stress below the critical one, what we call the exit-time. In figure 1(a) we schematically show the way we propose to estimate the breakup rate, using a real example taken from the evolution of one aggregate. In the figure, we show the time series of kinetic energy dissipation along an aggregate trajectory and the methodology followed to define the *exit-time*. An aggregate released at a time t_0 moves with the flow for a time $\tau_{\varepsilon_{\rm cr}}$ after which the local dissipation exceeds for the first time the critical threshold $\varepsilon_{\rm cr}$ (indicated by the dashed line in figure 1(a)) where the aggregate breaks up. The first crossing of $\varepsilon_{\rm cr}$ thus defines the exit-time, $\tau_{\varepsilon_{\rm cr}}$, which is the basic quantity for determining breakup rates.

For measuring the exit-time of aggregates, the following protocol is applied [29]: (i) At a time t_0 a given number of aggregates is released at a random location within a domain Ω of a stationary flow. (ii) Aggregates released at a point where the local dissipation exceeds $\varepsilon_{\rm cr}$ are ignored as breakup would have already occurred before the aggregate could have reached that point. (iii) The remaining aggregates are followed in time until the local dissipation exceeds the critical dissipation $\varepsilon_{\rm cr}$. The time

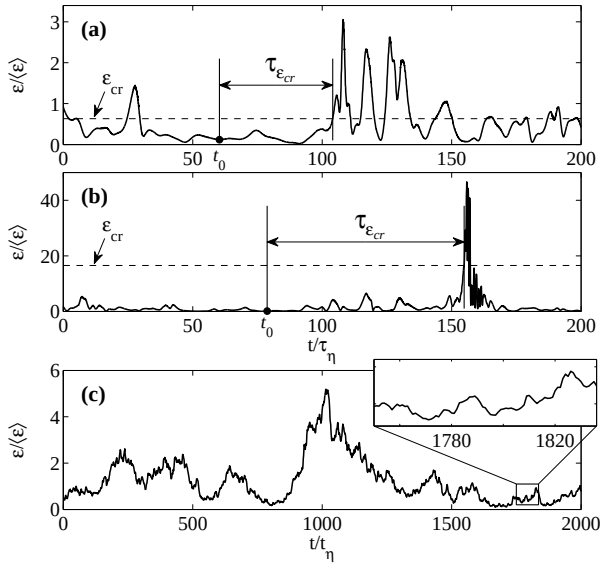

FIG. 1: Definition of the exit-time, $\tau_{\varepsilon_{\rm cr}}$ (see text) for two typical trajectories in a homogeneous and isotropic flow: (a) Time series of energy dissipation along an aggregate trajectory for a low-turbulent intensity trajectory; (b) the same but for a strongly turbulent burst. The dashed line indicates the critical dissipation. (c) A typical evolution of the energy dissipation for an aggregate evolving in a synthetic turbulent flow (STF). Notice the absence of strong fluctuations in the latter case. The horizontal axis is normalized by the Kolmogorov time scale $\tau_\eta = (\nu/\langle\varepsilon\rangle)^{1/2}$.

lag from release until the breakup defines the exit-time $\tau_{\varepsilon_{\rm cr}}$. The breakup rate for the given threshold and domain of release is then given by the inverse of the mean of the exit-time, given by the ensemble average over many time histories:

$$f_{\varepsilon_{\rm cr}} = \frac{1}{\langle \tau_{\varepsilon_{\rm cr}} \rangle}\,. \qquad (3)$$

Equation (3) provides a valid definition of the breakup rate that is applicable to both homogeneous and non-homogeneous flows. However, it is important to notice that its implementation requires to observe the particles for a sufficiently long time in order to confidently estimate the mean exit-time. This might be very challenging for measurements made in the field or in a laboratory, and for large values of $\varepsilon_{\rm cr}$ that occur only rarely. Hence, approximations to the breakup rate given by (3) are desirable. One of such approximation applicable to homogeneous flows is obtained by considering the *diving-time,* defined as the time lag in between two consecutive crossings of the critical dissipation [26]. The important difference obtained by using the diving-time is that in homogeneous flows the mean diving time can be obtained using the Rice theorem for the mean number of crossings per unit time of a differentiable stochastic process,

leading to the following proxy for the breakup rate [29]:

$$f^{(E)}_{\varepsilon_{\rm cr}} = \frac{\int_0^\infty \mathrm{d}\dot{\varepsilon}\ \dot{\varepsilon} p_2(\varepsilon_{\rm cr},\dot{\varepsilon})}{\int_0^{\varepsilon_{\rm cr}} \mathrm{d}\varepsilon\ p(\varepsilon)}\,, \tag{4}$$

where $p_2(\varepsilon,\dot{\varepsilon})$ is the joint probability density function (PDF) of the dissipation and its time derivate, $p(\varepsilon)$ is the PDF of ε, and the superscript (E) stands for 'Eulerian', indicating the fragmentation rate estimated without the need of Lagrangian properties.

Another important and potentially useful approximation can be derived by considering the evolution of the number of particles. In the case where breakup is driven by an uncorrelated force field, the breakup rate can be written as:

$$f^{(N)}_{\varepsilon_{\rm cr}} = -\frac{\mathrm{d}\ln N_{\varepsilon_{\rm cr}}(t)}{\mathrm{d}t}\,, \tag{5}$$

where $N_{\varepsilon_{\rm cr}}(t)$ is the number of aggregates at a time t after their release. The latter is simply related to the exit-time measurements described above by the relation,

$$N_{\varepsilon_{\rm cr}}(t)/N_{\varepsilon_{\rm cr}}(0) = 1 - \int_0^t \mathrm{d}\tau\ p_{\varepsilon_{\rm cr}}(\tau)\,, \tag{6}$$

where $N_{\varepsilon_{\rm cr}}(0)$ is the number of aggregates successfully released into the flow and $p_{\varepsilon_{\rm cr}}(\tau)$ is the PDF of the exit-time for a threshold $\varepsilon_{\rm cr}$.

Flow fields

Boundary layer flow

We consider a zero-pressure-gradient flow, i.e. the case of a thin flat plate immersed in a uniform steady stream of viscous fluid with undisturbed characteristic velocity U_0. No-slip boundary condition is applied on the flat plate. The viscous stresses generated by the flat plate retard the fluid elements close to the wall, so that the fluid zone close to the flat plate has a velocity lower than the free stream value U_0. The resulting flow is known as boundary layer flow (BLF). A sketch of the flow configuration is displayed in figure 2. A typical measure of the boundary layer thickness is the so called geometrical thickness δ, defined as the distance perpendicular to the wall where the flow reaches 99% of the undisturbed free-stream velocity. It is known from experiments and from simple dimensional arguments that the geometrical thickness increases when moving downstream along the flat plate, implying that the BLF is a spatially evolving flow with a strong inhomogeneity in the wall normal direction and a weaker evolution in the wall parallel directions. Different, though somehow equivalent measures of the characteristic boundary layer thickness exist such as the displacement thickness δ^* and the momentum thickness θ that take in account the mass and the momentum loss inside the boundary layer [38].

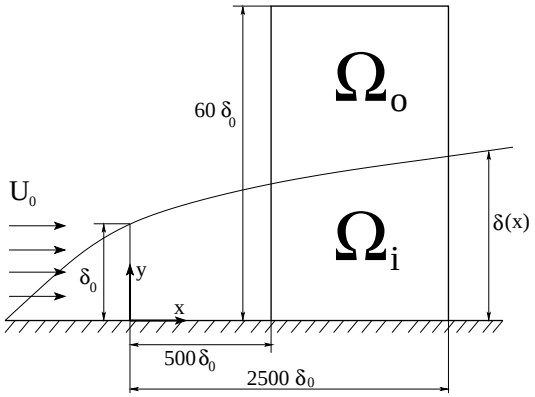

FIG. 2: Schematic of the BLF. The two different seeding regions are labeled as Ω_i for the aggregates released inside the boundary layer, and Ω_o for aggregates released outside the boundary layer region. $\delta(x)$ represents the geometric boundary layer thickness where the mean velocity is 99% of the free stream velocity U_0; δ_0 denotes the boundary layer thickness in the inlet section of the computational domain. x and y denote the streamwise and wall-normal coordinate, respectively.

A DNS of the BLF was performed using the pseudo-spectral Navier-Stokes solver SIMSON [39]. The computational domain has a size of $(3000\delta_0)\times(100\delta_0)\times(120\delta_0)$ in streamwise, wall-normal, and spanwise directions, with δ_0 denoting the geometrical boundary layer thickness at the inlet section of the computational domain. The numerical resolution is 4096×384 Fourier modes in the wall-parallel plane and 301 Chebishev modes in the wall-normal direction. A localized forcing, random in time and spanwise direction, close to the inlet is used to induce the laminar-turbulent transition. The characteristic Reynolds number of the flow, based on the momentum thickness θ, ranges from $Re_\theta = 200$ at the inlet to $Re_\theta = 2500$ at the end of the domain. The resulting turbulent flow is analogous to the one described in Sardina et al. [40, 41], where the transport and dispersion of inertial particles in boundary layers is studied.

Aggregates are released in two regions: inside the boundary layer (labeled Ω_i in figure 2) and outside the boundary layer (labeled Ω_o in figure 2). The release regions span the streamwise interval from $500\delta_0$ to $2500\delta_0$ such as to avoid interferences due to the tripping forcing promoting transition to turbulence. The height of the total release region is $60\delta_0$ and the difference between Ω_i and Ω_o is determined by the local geometrical thickness of the boundary layer. The latter ranges from $15\delta_0$ at the beginning of the release region to $45\delta_0$ at the end of the release region. A total number of 2×10^6 tracer aggregates is released into the flow. Aggregate trajectories are obtained by integrating the velocity field:

$$\frac{\mathrm{d}\boldsymbol{x}(t)}{\mathrm{d}t} = \boldsymbol{u}(\boldsymbol{x}(t),t)\,. \tag{7}$$

TABLE I: Parameters of the numerical experiments. ε_0 and τ_0 are the characteristic energy dissipation and the timescale used to normalize the data. In the BLF and CF aggregates are released in two regions: In the BLF, aggregates are released inside the boundary layer $\Omega_i = \{500 < x/\delta_0 < 2500, y < \delta(x)\}$, and outside the boundary layer $\Omega_o = \{500 < x/\delta_0 < 2500, \delta(x) < y < 60\delta_0\}$, where $\delta(x)$ and δ_0 are the boundary layer thickness and the boundary layer thickness at the entrance to the computational domain, respectively. In the CF, aggregates are released in the center-plane $\Omega_c = \{y/h = 0\}$ and in the wall region $\Omega_w = \{0.933 < |y/h| < 1\}$ where y is the wall normal coordinate and h is the half channel height.

Flow		Release region	ε_0	τ_0
BLF	$Re_\theta = 2500$	Ω_i, Ω_o	$\langle \varepsilon \vert \boldsymbol{x} \in \Omega_i \rangle$	$(\nu/\varepsilon_0)^{1/2}$
CF	$Re_\tau = 150$	Ω_c, Ω_w	$\langle \varepsilon \rangle$	$(\nu/\varepsilon_0)^{1/2}$
HIT	$Re_\lambda \simeq 400$	whole domain	$\langle \varepsilon \rangle$	$(\nu/\varepsilon_0)^{1/2}$
STF	$Re_\sigma = 300$	whole domain	$\langle \varepsilon \rangle$	t_η

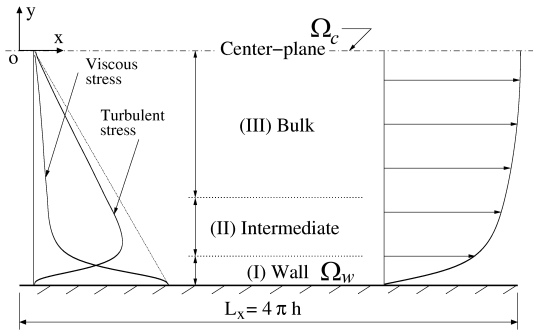

FIG. 3: Schematic of the CF. The two different seeding regions are labeled as Ω_c for aggregates released in the center-plane and Ω_w for aggregates released near the wall. On the left and right side are shown the mean profiles of turbulent and viscous stresses, and the mean velocity profile, respectively. h denotes the half channel height.

The fluid velocity and its spatial derivatives at the position of the aggregate are quantified by means of a fourth order spatial interpolation, while a second order Adams-Bashforth scheme is used for integration of (7). Further details about the numerics of the Lagrangian tracking solver can be found in Sardina et al. [40, 42]. The characteristic energy dissipation ε_0 used to normalize the breakup rate is taken as the volume average over the inner release region Ω_i. A summary of the properties of this flow is given in table I.

Channel flow

The flow domain consists of two infinite flat parallel plates, a distance $2h$ apart. The origin of the coordinate system is located at the center of the channel and x, y and z axes represent streamwise, wall-normal, and spanwise directions, respectively. Periodic boundary conditions are imposed on the fluid velocity field in homogeneous directions (x and z) while no-slip boundary conditions are imposed at the walls. The size of the computational domain is $L_x \times L_z \times L_y = 4\pi h \times 2\pi h \times 2h$. The flow is non-reactive, isothermal and incompressible (low Mach number). The shear Reynolds number is $Re_\tau = u_\tau h/\nu = 150$ [43], where $u_\tau = \sqrt{\tau_w/\rho}$ is the shear velocity based on the mean wall shear stress. The flow solver is based on the Fourier-Galerkin method in the streamwise and spanwise directions, and on a Chebishev-collocation method in the wall-normal direction. This solver provides the spatial derivatives required to calculate fluid dissipation along the aggregate trajectory according to (2) with spectral accuracy. A Lagrangian tracking code coupled with the flow solver is used to calculate the path of each aggregate in the flow. The aggregate equation of motion (7) is solved using a fourth-order Runge-Kutta scheme for time integration. Fluid velocity and velocity derivatives at aggregate position are obtained using sixth-order Lagrangian polynomials; at the wall, the interpolation scheme switches to one-sided. Further details on the numerical methodology can be found in Marchioli et al. [43] and Soldati and Marchioli [44]. A schematic of the flow is shown in figure 3.

Following Pitton et al. [45] the flow domain is phenomenologically divided in three regions, i.e. wall region, intermediate region, and bulk region (see figure 3). The wall region comprises a fluid slab with a thickness of 10 wall units. In this region, the viscous stress (representing the mean fluid shear) is maximum while the turbulent stress is close to zero. The intermediate region extends up to 50 wall units from the wall and is characterized by the peak of the fluid Reynolds stresses. The bulk region covers the central part of the channel where all wall stress contributions drop to zero and turbulence is closer to homogeneous and isotropic. Breakup experiments are performed by releasing aggregates in the wall region and at the center-plane of the bulk region. The two release regions are labeled Ω_w and Ω_c in figure 3. Within each of these release regions, 10^5 aggregates are released and their trajectories are tracked and breakup events are detected. The characteristic energy dissipation ε_0 used to normalize the breakup rate is taken as the volume average over the whole flow domain, see table I.

Homogeneous turbulence

A DNS of three-dimensional incompressible Navier-Stokes turbulence was performed on a triply periodic cubic box, with large scale statistically homogeneous and isotropic forcing. The external forcing injects energy in the first low wavenumber shells, by keeping their spectral content constant [46]. The kinematic viscosity is such that the Kolmogorov length-scale is comparable to

the grid spacing; this choice ensures a good resolution of the small-scale velocity dynamics. The Navier-Stokes equations are solved on a regular grid, 2π periodic, by means of standard pseudo-sprectal methods, with time stepping due to a second-order Adams-Bashforth algorithm. The grid has 2048^3 points and the Taylor scale based Reynolds number is $Re_\lambda \simeq 400$. Lagrangian particle velocities are obtained by a tri-linear interpolation. Details on the numerical integration can be found in Bec et al. [47]. The database for this study counts approximately 2×10^5 tracer trajectories. The the characteristic dissipation for normalizing the breakup rate, ε_0, is taken as mean dissipation, see table I.

Synthetic Flow

In order to better assess the importance of strong intermittent bursts in the statistics of the energy dissipation felt by the aggregates, it appears useful to study also the dynamical evolution in a *synthetic* turbulent flow (STF), whose statistics can be controlled a priori. This flow is built to mimic properties of stationary, homogeneous and isotropic turbulence, however with an important and crucial difference: with Gaussian statistics for the velocity field. The STF is realized in a three dimensional periodic box of size $L = 2\pi$ with the velocity field written as a Fourier series:

$$\boldsymbol{u}(\boldsymbol{x}, t) = \sum_{\boldsymbol{k}} \hat{\boldsymbol{u}}'_{\boldsymbol{k}}(t) e^{i\boldsymbol{k}\boldsymbol{x}} \,. \tag{8}$$

The Fourier coefficients obey $\hat{\boldsymbol{u}}'_{-\boldsymbol{k}} = \hat{\boldsymbol{u}}'^{*}_{\boldsymbol{k}}$; the star indicates the complex conjugate. The summation in (8) goes over $K = 1, \dots K_{\max}$ shells, each containing N_K uniformly distributed wave vectors of length $|\boldsymbol{k}| = K$. Incompressibility of $\boldsymbol{u}(\boldsymbol{x}, t)$ is ensured by taking $\hat{\boldsymbol{u}}'_{\boldsymbol{k}}$ as the projection of a different vector $\hat{\boldsymbol{u}}_{\boldsymbol{k}}$ on a plane perpendicular to $\boldsymbol{k}$. The vector $\hat{\boldsymbol{u}}_{\boldsymbol{k}}$ is evolved by a second order stochastic process, originally proposed by Sawford [48] to model Lagrangian dispersion. Evolving $\hat{\boldsymbol{u}}_{\boldsymbol{k}}$ by a second order stochastic process results in a velocity field that is differentiable in time, which is a crucial property for measuring temporal statistics such as the exit-time. In the second order process, the spectral acceleration $\hat{\boldsymbol{a}}_{\boldsymbol{k}}$ is given by the following stochastic differential equation:

$$\mathrm{d}\hat{\boldsymbol{a}}_{\boldsymbol{k}} = -\frac{\hat{\boldsymbol{a}}_{\boldsymbol{k}}}{t_\eta}\mathrm{d}t - \frac{\hat{\boldsymbol{u}}_{\boldsymbol{k}}}{t_\eta t_L}\mathrm{d}t + \sqrt{\frac{2\sigma^2_{\boldsymbol{k}}}{t^2_\eta t_L}}\mathrm{d}\boldsymbol{W} \,, \tag{9}$$

where $\mathrm{d}\boldsymbol{W}$ is an incremental Wiener process, t_η and t_L are the timescales of acceleration and velocity, respectively, and $\sigma^2_{\boldsymbol{k}}$ is the variance of a component of $\hat{\boldsymbol{u}}_{\boldsymbol{k}}$. Due to the isotropy of the flow field, $\sigma^2_{\boldsymbol{k}}$ depends only on the modulus of $\boldsymbol{k}$, i.e. $\sigma^2_{\boldsymbol{k}} = \sigma^2_K$, such that the energy carried by all wave vectors of modulus K is $E_K = \frac{3}{2} N_K \sigma^2_K$, and the total energy is $E = \frac{3}{2}\langle u^2 \rangle = \sum_{K=1}^{K_{\max}} E_K$. The spectral velocity $\hat{\boldsymbol{u}}_{\boldsymbol{k}}$ is simply:

$$\mathrm{d}\hat{\boldsymbol{u}}_{\boldsymbol{k}} = \hat{\boldsymbol{a}}_{\boldsymbol{k}}\mathrm{d}t \,. \tag{10}$$

In the present simulations, we set $K_{\max} = 1$ [49, 50] and take the mean velocity $\langle u^2 \rangle^{1/2}$ small with respect to L/t_L. For this choice of parameters, the Lagrangian properties are fully determined by the evolution of the spectral coefficients. Following Sawford [48], the spectral acceleration decorrelates with $\sim t_\eta$ while the integral scale of the spectral velocity is equal to t_L. This allows for interpreting t_η as the equivalent of the dissipative time scale in turbulence, and furthermore, it motivates to estimate a small-scale Reynolds number for the STF, denoted as Re_σ, as [48]:

$$Re_\sigma \sim t_L / t_\eta \,, \tag{11}$$

In this work, we set $Re_\sigma = 300$ and use t_η as the characteristic time scale for normalizing the breakup rate; the characteristic dissipation ε_0 is taken as the mean dissipation (table I). Like in the other flows, the aggregate trajectory is obtained by integrating the velocity field, (8), while the local dissipation is obtained from (2), setting the value of the viscosity equal to unity. For measuring breakup rates, several very long trajectories were simulated from which we then measured diving- times. From the diving-time, the mean exit-time was obtained from an exact relation derived in Babler et al. [29]. The breakup rate determined this way corresponds to the case were aggregates are released homogeneously in the whole domain. The statistical database is as large as 1.5×10^6 diving events.

Before concluding this section, it is worthwhile stressing the main differences between the STF presented here and a realistic turbulent flow. First, even though we can identify two different time scales in the STF, the dissipation along an aggregate trajectory in STF will not possess any anomalous and intermittent scaling, see e.g. Biferale et al. [51]. Second, the spatial configuration of the STF is smooth and does not exhibit a Kolmogorov-like $-5/3$ spectrum. The former is particularly relevant and will be discussed later in connection to the small efficiency of the STF to break strong aggregates.

RESULTS

Properties of energy dissipation

Energy dissipation plays a decisive role in the breakup of small aggregates. In this section we therefore first explore the Lagrangian and Eulerian properties of energy dissipation in the considered flows.

Figure 4 shows typical trajectories of tracer-like aggregates in the BLF. Panel (*a*) shows time series of the

wall normal distance while panel (b) shows the corresponding local dissipation. Among the three trajectories shown, A and B are cases of aggregates released inside the boundary layer, while C is a case of an aggregate released outside the boundary layer. Within the observed time lag, aggregate A is subject to strong fluctuations in dissipation that increase as it moves downstream and as the aggregate comes closer to the wall. On the other hand, aggregate B is first repelled from the boundary layer and moves away from the wall. Accordingly, the dissipation decreases and fluctuations are rarer. Later, the aggregate is re-entrained into the boundary layer, which causes dissipation to increase both in magnitude and amplitude of fluctuations. The trajectory of aggregate B in this later stage is thus similar to aggregate C that is entrained into the boundary layer after moving downstream for a certain distance. From these apparently ad-hoc examples it becomes clear that in the presence of a mean flow, breakup events will be controlled by an interplay between the mean flow properties and the relative fluctuations around it. For some aggregate histories the mean profile will control the breakup process, while for others, breakup is controlled by intense fluctuations of the local energy dissipation around its mean value. As seen below, the balance between the two strongly depends on the geometry of the flow configuration, the intensity of the turbulent fluctuations, and also on where the aggregates are released.

The above discussion can be quantified by looking at the time-averaged profiles of the energy dissipation in the BLF measured at three downstream distances as shown by figure 5, for the mean flow and the fluctuating components. Close to the wall, dissipation assumes large values that are dominated by the mean flow, as shown by the solid curves in figure 5. Dissipation due to turbulent velocity fluctuations (dashed curves) exhibits a flatter profile that expands well beyond the boundary layer thickness δ^*. The decrease of dissipation in the streamwise direction is small, as shown in the inset of figure 5 where we plot the time averaged dissipation at the wall as a function of Re_θ. This explains the relatively constant high magnitude of energy dissipation seen by an aggregate moving within the boundary layer (i.e. trajectory A in figure 4).

Figures 6 and 7 show analogue data for the CF. Here, aggregate A and B are released in the center-plane of the channel while aggregate C and D are released in the wall region. The aggregates released in the center-plane gradually get entrained by turbulent eddies which transport them to the walls. The entrainment and transport to the wall causes an increase in the magnitude of dissipation seen by the aggregate while fluctuations remain persistent. Once they reach the wall, the aggregates have the tendency to stay there for a relatively long time before being re-ejected into the bulk flow. This is seen also for aggregates released close to the wall where aggregate D

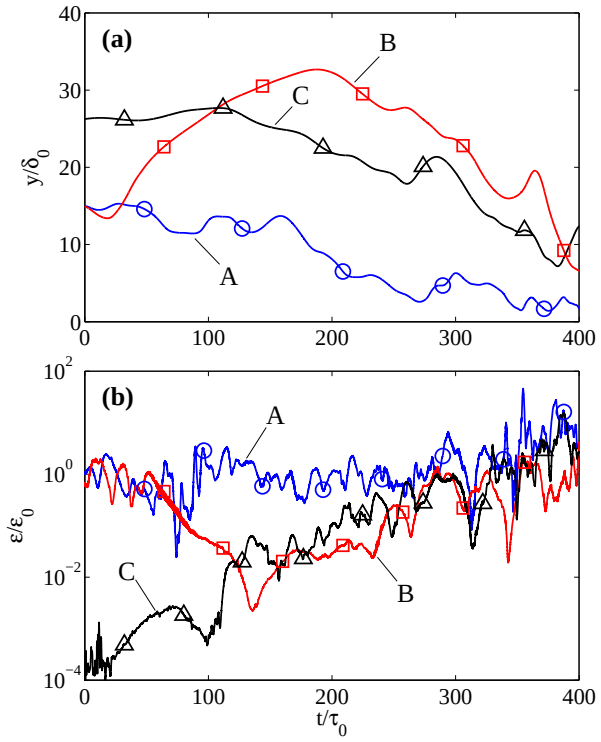

FIG. 4: Time series of (a) wall normal distance and (b) energy dissipation along typical aggregate trajectories in BLF. Trajectory A and B refer to aggregates released in Ω_i, while trajectory C refers to an aggregate released in Ω_o (see figure 2). Axis are normalized by ε_0 and τ_0 given in table I.

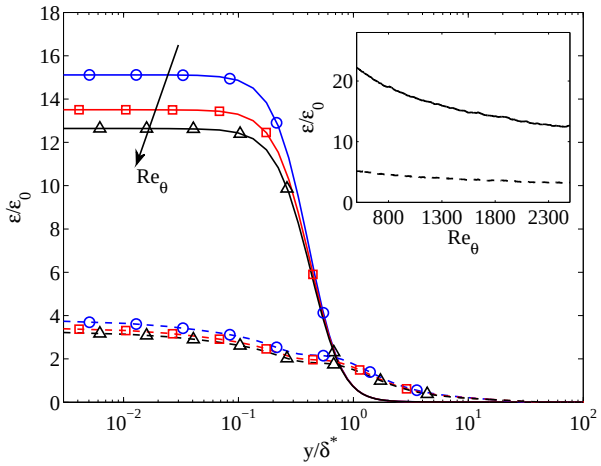

FIG. 5: Time averaged energy dissipation in BLF as a function of the wall normal distance at three downstream positions, characterized by Re_θ = 1700, 2100, and 2500, respectively. Solid lines: dissipation due to the mean flow, dashed lines: dissipation due to velocity fluctuations. The horizontal axis is normalized by the displacement thickness δ^*, while the vertical axis is normalized by ε_0 given in table I. Inset: Time averaged energy dissipation at the wall as a function of Re_θ representing the streamwise direction. Solid and dashed lines have the same meaning as the main axes.

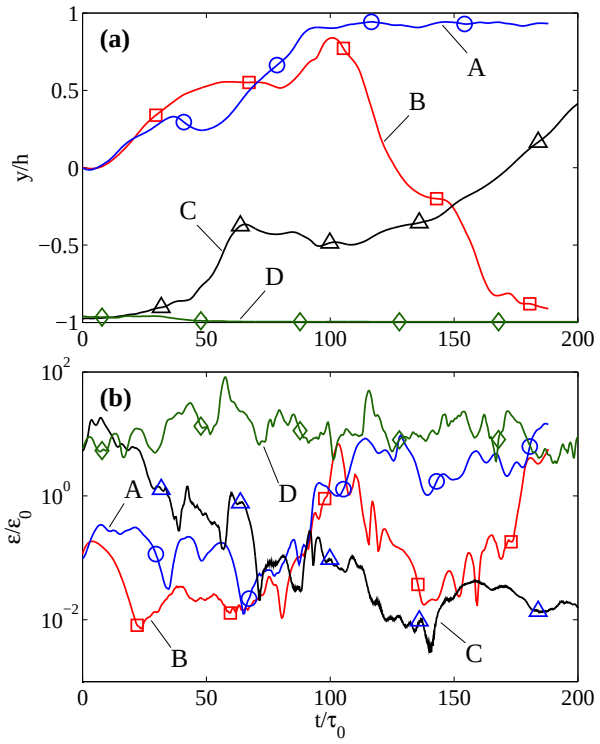

FIG. 6: Time series of (a) wall normal distance and (b) energy dissipation along typical aggregate trajectories in CF. Trajectory A and B refer to aggregates released in Ω_c, while trajectory C and D refer to aggregates released in Ω_w (see figure 3). Axis are normalized by ε_0 and τ_0 given in table I.

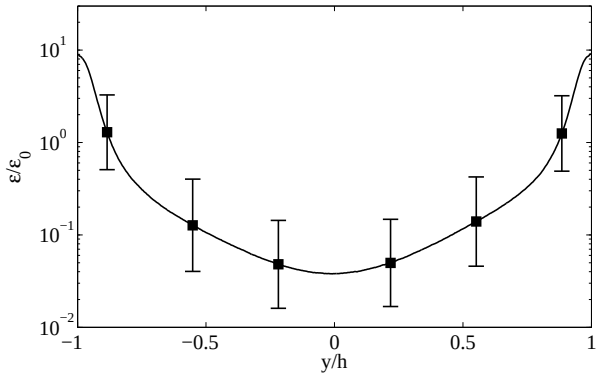

FIG. 7: Mean energy dissipation conditioned on the wall normal distance in the CF. Error bars indicate the root-mean-square of the conditioned dissipation. The vertical axis is normalized by ε_0 given in table I.

stays close to the wall while aggregate C is ejected into the bulk flow. As it appears in figure 7, where we plot the mean dissipation conditioned on the wall normal distance, aggregates are subject to high fluctuations of the kinetic energy dissipation even when staying in the bulk flow (i.e. away from the walls). Likewise to the BLF, dissipation assumes high values close to the walls while fluctuations in dissipation, indicated by error bars, are intense throughout the channel.

We now consider homogeneous flows. Let us go back to the time series of dissipation along tracer trajectories in HIT shown in figure 1. Panel (a) shows a *calm trajectory*, i.e. a time interval during which dissipation undergoes moderate fluctuations around the mean. On the other hand, panel (b) shows a trajectory that experiences strong intermittency, i.e. the dissipation undergoes sudden bursts during which its value for a short time exceeds the average dissipation by several standard deviations [52]. Such bursts in dissipation are caused by trapping of particles in intense but short lived vortex structures [51], which create very high velocity gradients and which, as shown bellow, have a distinct influence on the breakup of strong aggregates.

Panel (c) in figure 1 reports the behavior of the dissipation along a tracer trajectory in STF. The panel shows the dissipation over a time interval of $2000 \times t_\eta$, from which it is seen that the signal is controlled by two timescales, namely t_η that controls the fast fluctuations and t_L that controls the slow fluctuations. Magnifying the time series, as done in the inset of panel (c), highlights the correspondence of the fast fluctuations in the smooth flow to the fine scale fluctuations in the homogeneous and isotropic turbulent flow. Also, the time series of dissipation in the synthetic flow describes a much more regular signal when compared to turbulence, i.e. intermittent bursts and strong deviations from the mean are absent in this flow. As shown in the next section, this limits the capability of the STF to break strong aggregates.

Finally, the Eulerian PDF of the energy dissipation of the homogenous flows are shown in figure 8, together with the dissipation PDF of the CF. In agreement with other studies [53, 54], the dissipation PDF of the HIT for the given Reynolds number exhibits a left tail that is close to log-normal and a peak value that is slightly smaller than the mean dissipation. In comparison, the dissipation PDF of the STF is much narrower. Lastly, the dissipation PDF of the CF is very wide as a consequence of the non-homogeneity of the flow. The PDF indeed exhibits two pronounced shoulders corresponding to the values of ε in the bulk (left shoulder) and in the wall regions (right shoulder).

Breakup rate measurements

We now have all the ingredients to measure and rationalize the breakup rates in turbulent flow at changing the turbulent intensity and the mean flow configuration. Results are summarized in figure 9 which marks the major result of this work. In figure 9 we report the measured

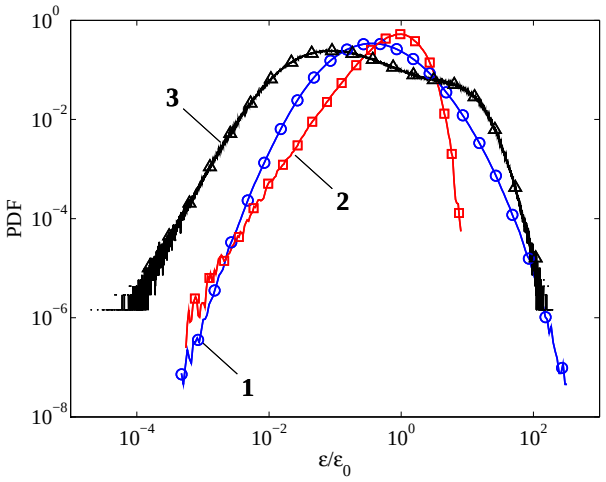

FIG. 8: Log-log plot of the PDFs of energy dissipation in (1) HIT, (2) STF, and (3) CF. The vertical axis is normalized by ε_0 given in table I, which for the shown flows refers to the volume average, respectively the mean.

breakup rates at changing the flow configuration, the release region, and the method used to estimate $f_{\varepsilon_{\rm cr}}$. We stress that to the best of our knowledge this is the first attempt to perform such comprehensive compilation on such a wide set of flow configurations. Additionally, we also report results from independent predictions, namely the estimate obtained from quasi-Eulerian measurements given in (4) or the approximation based on an exponential fit given in (5). As expected, the breakup rate generally decreases with increasing aggregate strength, confirming earlier results that large aggregates break faster than small ones. Remarkably, except data from the BLF where aggregates were released outside the boundary layer region, the breakup rates of the different flows are very close to each other for small threshold values. We stress that this is not due to a rescaling of the axis, but instead a consequence of using the characteristic dissipation ε_0 and its corresponding timescale for normalizing the axis.

Furthermore, for small $\varepsilon_{\rm cr}$ the breakup rate shows a power-law like behavior that is similar among the different datasets. To explore this further, in the inset of figure 9 we show the compensated breakup rate $f_{\varepsilon_{\rm cr}}/[\varepsilon_{\rm cr}^{-\chi}]$ using a scaling exponent $\chi = 0.42$. The latter corresponds to a fit of the right tail of the quasi-Eulerian proxy (4) which well describes breakup in HIT, as shown by the solid curve in figure 9. A clear plateau can be observed for aggregates released close the wall and for aggregates in homogeneous flows. Deviations from the plateau are only seen for aggregates released in the centerline of channel and for aggregates released outside the boundary layer for which the breakup rate for small $\varepsilon_{\rm cr}$ has a slightly larger scaling exponent. For these release regions, the aggregates first get entrained by turbulent eddies that transport them to the wall. During this entrainment the aggregates gradually experience stronger stress (cf. trajectory A in figure 5). Weak aggregates therefore, on average, will suffer breakup earlier than stronger ones, which causes the breakup rate for these release regions to decrease faster with increasing $\varepsilon_{\rm cr}$.

For larger thresholds values, a leveling-off in the decrease of the breakup rate is observed for the wall-bounded flows and $f_{\varepsilon_{\rm cr}}$ is found to bend upwards. This is in contrast to the homogenous flows for which $f_{\varepsilon_{\rm cr}}$ shows a strong drop-off at large $\varepsilon_{\rm cr}$ [29]. The higher breakup rates for wall-bounded flows are due to the high mean shear close to the wall which causes aggregates coming close to the wall to rapidly breakup. In the homogenous flows, strong aggregates are only broken by the rare excursions of dissipation from the mean caused by intermittency. As these events are rare, the breakup rate exhibits a super-exponential drop-off for large dissipation. In the STF, where strong and intermittent excursions from the mean are absent, the drop-off of the breakup rate occurs at much smaller thresholds values than in the case of HIT. The differences for high threshold values between the STF and real homogeneous and isotropic turbulence reflects the intriguing dynamics of turbulent fluctuations and the difficulty of modeling them. Indeed, only for these two cases the statistics of aggregate breakup is high enough to allow us to assess the super-exponential drop-off and thus to see the importance of turbulence: extremely robust aggregates break only due to the occurrence of corresponding extremely intense fluctuations, typical of the intermittent nature of small-scale turbulent flows. Any stochastic surrogate failing to possess this critical features would strongly overpredict the breakup rate, as it is the case for the STF analyzed here.

For very large threshold values, a drop-off in the breakup rate is also seen for the channel flow where the aggregates are released close the wall. It represents the case where the aggregates are too strong to be broken by the mean shear, and only intense but rare turbulent fluctuations within the near wall region are able to overcome the aggregate strength. A similar drop-off is likely to occur also for the other cases if trajectories were followed long enough. Exploring this region of high threshold values presents a problem for future work. In addition, figure 9 shows the breakup rate of the exponential model of Kusters [27] (dashed curve). This model is based on a simple dimensional assumption that breakup is ruled by Gaussian energy dissipation fluctuations:

$$f_{\varepsilon_{\rm cr}}^{(K)} = \frac{(4/15\pi)^{1/2}}{(\nu/\langle\varepsilon\rangle)^{1/2}} \exp(-15/2\ \varepsilon_{\rm cr}/\langle\varepsilon\rangle). \qquad (12)$$

The exponential model predicts a very sharp drop-off at intermediate threshold values and a constant breakup rate for small threshold values in strong disagreement to the breakup rate found in the simulations. The discrepancy originates mainly from the simplified assumption of

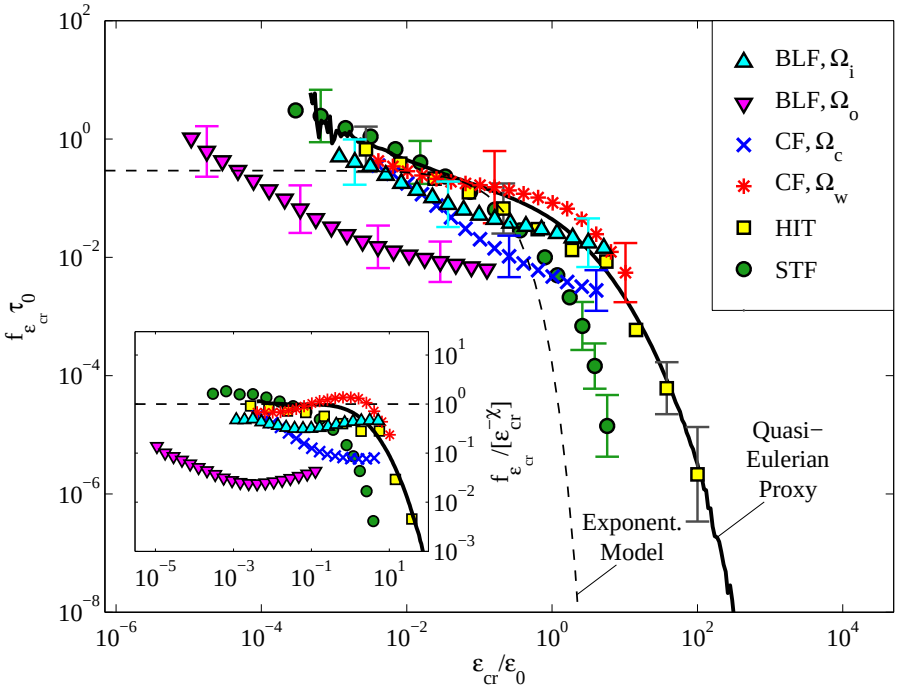

FIG. 9: Breakup rate as a function of the critical dissipation. Symbols: exit-time measurements in a given flow configuration and release region (see table I); the last three points on the right for the HIT data represent estimates from the decay of the number of aggregates according to (5). Solid line: quasi-Eulerian proxy to HIT (4); dashed line: exponential model (12). Inset: Compensated breakup rate $f_{\varepsilon_{\rm cr}}/[\varepsilon_{\rm cr}^{-\chi}]$ with $\chi = 0.42$ [29]. Symbols have the same meaning as in the main axis.

a Gaussian dissipation.

The observation made in figure 9 suggest that weak aggregates in the wall-bounded flows are broken by turbulent fluctuations shortly after their release, while on the other hand, strong aggregates survive for a longer time during which they move further downstream where they eventually suffer breakup due to the mean shear. To explore this further, we examined the spatial location at which breakup occurs in the wall-bounded flows. Two cases are considered: aggregates released inside the boundary layer of the BLF (figure 10) and aggregates released in the center-plane of the CF (figure 11). Figure 10 shows the average streamwise and wall normal coordinates at which breakup occurs for different threshold values. As it can be seen, with increasing threshold the aggregates on average move further downstream and come closer to the wall before suffering breakup. The average breakup location of weak aggregates thereby is close to the average location of where the aggregates were released. Figure 11 shows the PDF of the breakup location in the CF for three different threshold values. As it can be seen, weak aggregates predominantly break in the bulk of the channel close to the point of release, while strong aggregates move further downstream and predominantly break close to the wall. This observation is important for applications, and might open a way to tailor turbulent filters with different selecting properties depending on the

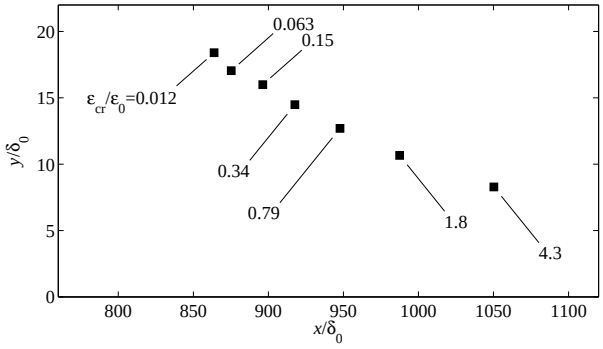

FIG. 10: Average (x, y)-coordinates of the breakup position for different threshold values of aggregates released in Ω_i in the BLF (see figure 2).

spatially evolving intensity of the turbulent background.

Evolution of the number of aggregates

Strong aggregates can move away from the point of release towards the high shear zones close to the walls: this fact has a clear influence on the breakup behavior, and leads to the high breakup rates at large threshold values in wall bounded flows (cf. figure 9). This preferential

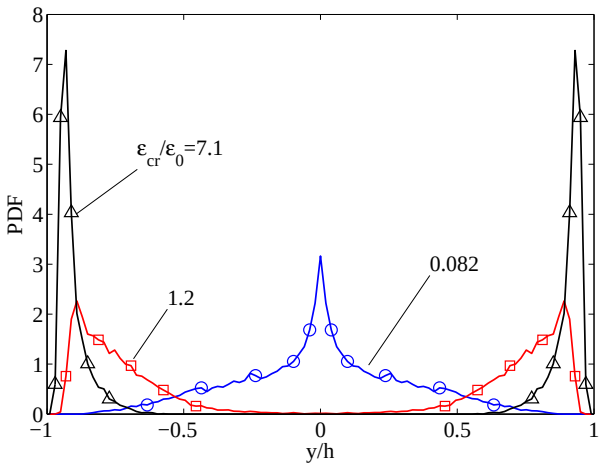

FIG. 11: Distribution of the wall normal distance where breakup occurs in CF for aggregates released in Ω_c (see figure 3). Different curves refer to different values of the critical dissipation.

breakup in specific regions of the flow is also reflected in the time evolution of the number of aggregates, $N_{\varepsilon_{\rm cr}}(t)$, present in the suspension. From (6), it is understood that $N_{\varepsilon_{\rm cr}}(t)$ is proportional to the cumulative exit-time distribution. As in the previous section, we limit the discussion to three cases, namely aggregates released inside the boundary layer in the BLF, aggregates released in the center-plane in the CF, and aggregates released in HIT. Not shown is the time evolution in the STF for which the time evolution of the number of aggregates shows the expected result of a Poisson process.

In figure 12(a), the evolution of the number of aggregates released inside the boundary layer in the BLF is reported. The figure shows $N_{\varepsilon_{\rm cr}}(t)$ in semi-logarithmic coordinates, with the different curves referring to different threshold values. It is clear that for small threshold values (lower curves in figure 12(a) the number of aggregates decays exponentially as $N_{\varepsilon_{\rm cr}}(t) \simeq N_0 \exp(-f^{(N)}_{\varepsilon_{\rm cr}} t)$, while deviations from the exponential decay observed at late times are due to statistical noise as the number of aggregates is already very small. The slope $f^{(N)}_{\varepsilon_{\rm cr}}$, as suggested by (5), provides an estimate of the breakup rate. The exponential decay represents the case where the aggregates are broken by uncorrelated turbulent fluctuations in the vicinity of the point of release. On the other hand, for large threshold values (upper curves in figure 12(a), the evolution of the number of aggregates shows a different pattern: after an exponential decay at short times, a relaxation sets in at intermediate times which eventually turns into an abrupt decrease at later times. Among these three stages, the relaxation stage following the exponential decay of $N_{\varepsilon_{\rm cr}}(t)$ is caused by aggregates surviving early breakup and moving away from the point of release. However, later, when these aggregates come close to wall they suffer abrupt breakup as represented by the third stage.

The good news here is that despite such non trivial time evolution, estimating the breakup rate from the linear segments of $\ln N_{\varepsilon_{\rm cr}}(t)$ provides a reasonable approximation. This is shown in the inset of figure 12(a) where we compare the breakup rate measured by the mean exit-time, as plotted in figure 9, with the estimation from the linear segments. The latter is very close to the former, which implies that for the considered threshold values the rate of breakup in the BLF is controlled by the early breakup events in the vicinity of the point of release of the aggregates.

The evolution of the number of aggregates released in the center-plane of the CF is shown in figure 12(b). As in the case for the BLF, for small threshold values (lower curves in figure 12(b)) the number of aggregates decays exponentially, implying that the aggregates are broken by short-time correlated turbulent fluctuations in the vicinity of the point of release. On the other hand, for large threshold values (upper curves in figure 12(b)), the evolution of $N_{\varepsilon_{\rm cr}}(t)$ is delayed and its decay only sets in after the aggregates have been in the flow for a certain time. This delay reflects the time it takes for the aggregates to get entrained into turbulent eddies which transport them to the higher shear regions close to the wall, where they eventually suffer breakup. The breakup rate estimated from fitting the linear segments of $\ln N_{\varepsilon_{\rm cr}}(t)$ is shown in the inset of figure 12(b), together with the exact breakup rate from exit-time measurements as plotted in figure 9. A good agreement with the exact breakup rate is observed also in this case.

Lastly, the evolution of the number of aggregates in HIT is shown in figure 12(c). In contrast to the wall bounded flows, no qualitative difference in the decay of $N_{\varepsilon_{\rm cr}}(t)$ for different threshold values is seen, and for all threshold values an exponential decay is observed, as indicated by the dashed lines. The breakup rate estimated from this initial decay is shown in the inset of figure 12(c), together with the exact breakup rate from figure 9. The latter is available up to threshold values $\varepsilon_{\rm cr}/\langle\varepsilon\rangle \sim 5$; beyond this value, exit-times are large compared with the duration of our numerical simulation which precludes exact measurements of the breakup rate. As it can be seen from the inset, for threshold values smaller than $\varepsilon_{\rm cr}/\langle\varepsilon\rangle \sim 5$ the approximated breakup rate is very close to the exact breakup rate, while for larger threshold values it is in good agreement with the *quasi*-Eulerian proxy shown by the solid curve. This close agreement indicates that breakup in HIT resembles breakup in short-time correlated force field which justifies modeling breakup as a first order rate process.

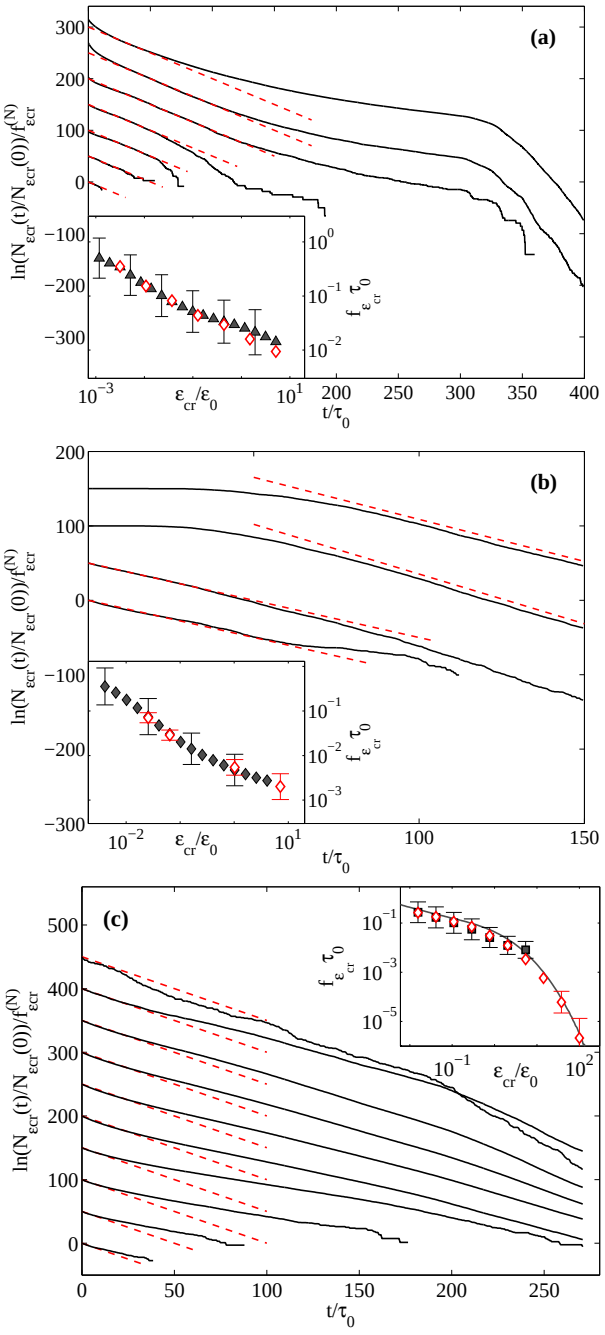

FIG. 12: Evolution of the number of aggregates in semi-logarithmic coordinates for (a) BLF with aggregates released in Ω_i, (b) CF with aggregates released in Ω_c, and (c) HIT. Main axes: $\ln(N_{\varepsilon_{cr}}(t)/N_{\varepsilon_{cr}}(0))$ for different threshold values normalized by the slope $f^{(N)}_{\varepsilon_{cr}}$ of the pure exponential decay. For clarity, the curves are shifted upwards by a fixed increment such that ε_{cr} increases from bottom to top. The dashed lines indicate the linear regions used to fit $f^{(N)}_{\varepsilon_{cr}}$. Inset: Breakup rate as a function of critical dissipation obtained from exit-time measurements (solid symbols) and linear fits to $\ln N_{\varepsilon_{cr}}(t)$ (open symbols). The former is the same as data plotted in figure 9. The solid line in inset (c) shows the quasi-Eulerian proxy (4).

CONCLUSIONS

We reported the first systematic study concerning the estimation of the breakup rate of small aggregates in fully developed turbulence at changing both the flow configuration (bounded and unbounded) and the injection region (relevant only for the bounded-flow cases). Also, we discussed theoretical and phenomenological ideas concerning the definition of the breakup rate in terms of the so-called exit-times measured along the trajectories of all aggregates, or in terms of other proxies, e.g. breakup rates defined in terms of fully Eulerian quantities or using a fast-decorrelation hypothesis along Lagrangian trajectories. Our main approximations are the assumption that breakup occurs instantaneously once the dissipation at the position of the aggregate exceeds a predefined threshold value, and that only one-way coupling is considered (no feedback on the flow). In future work, the former restriction could be overcome by considering certain time-relaxation properties of the aggregate backbone.

We found that breakup is typically the results of two competing effects: a systematic influence of the mean turbulent profile, overlaid by intermittent and bursty events induced by turbulent fluctuations. In turbulent regions dominated by small dissipation events, important for large and easy-to-break aggregates, the breakup rate shows a similar pattern in all considered flows. In particular we found that the breakup rate in the different flows exhibits a qualitative similar power law scaling. This is explained by noticing that weak aggregates are broken by turbulent fluctuations in the vicinity of the point of release. As the local properties of turbulence at the injection point are expected to be similar, in dimensionless units, the breakup rate assumes similar values.

On the other hand, breakup rates driven by large dissipation events are significantly different among the four flows. Compared to homogeneous isotropic turbulence, the bounded flows lead to much higher breakup rates for large values of the threshold dissipation. This is due to the fact that in non-homogeneous flows, aggregates might be broken also by the mean flow if they travel enough to reach regions close to the boundary. On the contrary, the synthetic turbulent flow shows very small breakup rates for large threshold dissipations due to the absence of both a mean profile and intense intermittent fluctuations, characteristic of realistic homogeneous and isotropic turbulent flows.

The study presented here can be seen as the first step towards the systematic development of models for aggregation kernels and breakup rates to be used in spatially distributed population balances and compartment models.

Acknowledgments

Computer time provided by SNIC, Swedish National Infrastructure for Computing, and technical support from CINECA is gratefully acknowledged. M.U.B. was financially supported by the Swedish Research Council VR (No 2012-6216). L.B. acknowledges partial funding from the European Research Council under the European Community's Seventh Framework Program, ERC Grant Agreement No 339032. EU-COST action MP0806 is kindly acknowledged.

* Electronic address: babler@kth.se

[1] K. A. Kusters, J. G. Wijers, and D. Thoenes, Chem. Eng. Sci. **52**, 107 (1997).
[2] M. U. Babler, A. S. Moussa, M. Soos, and M. Morbidelli, Langmuir **26**, 13142 (2010).
[3] B. K. Brunk, D. L. Koch, and L. W. Lion, J. Fluid Mech. **364**, 81 (1998).
[4] W. C. Reade and L. R. Collins, J. Fluid Mech. **415**, 45 (2000).
[5] J. C. Flesch, P. T. Spicer, and S. E. Pratsinis, AIChE J. **45**, 1114 (1999).
[6] M. Kobayashi, Y. Adachi, and O. Setsuo, Langmuir **15**, 4351 (1999).
[7] J. J. Derksen, AIChE J. **58**, 2589 (2012).
[8] C. Selomulya, G. Bushell, R. Amal, and T. D. Waite, Langmuir **18**, 1974 (2002).
[9] Y. Yuan and R. R. Farnood, Powder Technol. **199**, 111 (2010).
[10] P. Bubakova, M. Pivokonsky, and P. Filip, Powder Technol. **235**, 540 (2013).
[11] T. Li, Z. Zhu, D. S. Wang, C. H. Yao, and H. X. Tang, Powder Technol. **168**, 104 (2006).
[12] M. Soos, A. S. Moussa, L. Ehrl, J. Sefcik, H. Wu, and M. Morbidelli, J. Colloid Interface Sci. **319**, 577 (2008).
[13] C. Biggs, P. Lant, and M. Hounslow, Water Sci. Tech. **47**, 251 (2003).
[14] A. Zaccone, M. Soos, M. Lattuada, H. Wu, M. U. Babler, and M. Morbidelli, Phys. Rev. E **79**, 061401 (2009).
[15] B. Ó Conchúir and A. Zaccone, Phys. Rev. E **87**, 032310 (2013).
[16] A. A. Potanin, J. Colloid Interface Sci. **157**, 399 (1993).
[17] M. L. Eggersdorfer, D. Kadau, H. J. Herrmann, and S. E. Pratsinis, J. Colloid Interface Sci. **342**, 261 (2010).
[18] R. C. Sonntag and W. B. Russel, J. Colloid Interface Sci. **113**, 399 (1986).
[19] M. Soos, L. Ehrl, M. U. Babler, and M. Morbidelli, Langmuir **26**, 10 (2010).
[20] Y. M. Harshe, M. Lattuada, and M. Soos, Langmuir **27**, 5739 (2011).
[21] C. Selomulya, G. Bushell, R. Amal, and T. D. Waite, Chem. Eng. Sci. **58**, 327 (2003).
[22] M. U. Babler and M. Morbidelli, J. Colloid Interface Sci. **316**, 428 (2007).
[23] M. Soos, J. Sefcik, and M. Morbidelli, Chem. Eng. Sci. **61**, 2349 (2006).
[24] J. Maerz, R. Verney, K. Wirtz, and U. Feudel, Cont. Shelf Res. **31**, S84 (2011).
[25] M. A. Delichatsios, Phys. Fluids **18**, 622 (1975).
[26] V. I. Loginov, J. Appl. Mech. Tech. Phys. **26**, 509 (1985).
[27] K. A. Kusters, *The influence of turbulence on aggregation of small particles in agitated vessels* (PhD Thesis, Technische Universiteit Eindhoven, 1991).
[28] M. U. Babler, M. Morbidelli, and J. Baldyga, J. Fluid Mech. **612**, 261 (2008).
[29] M. U. Babler, L. Biferale, and A. S. Lanotte, Phys. Rev. E **85**, 025301 (2012).
[30] J. De Bona, A. S. Lanotte, and M. Vanni, submitted to J. Fluid Mech. (2013).
[31] E. Balkovsky, A. Fouxon, and V. Lebedev, Phys. Rev. Lett. **84**, 4765 (2000).
[32] L. Biferale, C. Meneveau, and R. Verzicco, submitted to J. Fluid Mech. (2014).
[33] P. Maffettone and M. Minale, J. Non-Newton Fluid **78**, 227 (1998).
[34] Y. M. Harshe and M. Lattuada, Langmuir **28**, 283 (2012).
[35] V. Becker, E. Schlauch, M. Behr, and H. Briesen, J. Colloid Interface Sci. **339**, 362 (2009).
[36] M. Vanni and A. Gastaldi, Langmuir **27**, 12822 (2011).
[37] M. Soos, R. Kaufmann, R. Winteler, M. Kroupa, and B. Luthi, AIChE J. **59**, 3642 (2013).
[38] H. Schlichting, *Boundary-layer theory*, vol. 539 (McGraw-Hill New York, 1968).
[39] M. Chevalier, P. Schlatter, A. Lundbladh, and D. S. Henningson, Tech. Rep. TRITA-MEK 2007:07, KTH Mechanics (2007).
[40] G. Sardina, P. Schlatter, F. Picano, C. M. Casciola, L. Brandt, and D. S. Henningson, J. Fluid Mech. **706**, 584 (2012).
[41] G. Sardina, F. Picano, P. Schlatter, L. Brandt, and C. M. Casciola, Flow Turbul. Combust. **92**, 27 (2014).
[42] G. Sardina, P. Schlatter, L. Brandt, F. Picano, and C. M. Casciola, J. Fluid Mech. **699**, 50 (2012).
[43] C. Marchioli, A. Soldati, J. G. M. Kuerten, B. Arcen, A. Taniere, G. Goldensoph, K. D. Squires, M. F. Cargnelutti, and L. M. Portela, Int. J. Multiphase Flow **34**, 879 (2008).
[44] A. Soldati and C. Marchioli, Int. J. Multiphase Flow **34**, 879 (2009).
[45] E. Pitton, C. Marchioli, V. Lavezzo, A. Soldati, and F. Toschi, Phys. Fluids **24**, 073305 (2012).
[46] S. Chen, G. D. Doolen, R. H. Kraichnan, and Z.-S. She, Phys. Fluids A **5**, 458 (1993).
[47] J. Bec, L. Biferale, A. S. Lanotte, A. Scagliarini, and F. Toschi, J. Fluid Mech. **645**, 497 (2010).
[48] B. L. Sawford, Phys. Fluids A **3**, 1577 (1991).
[49] J. Bec, J. Fluid Mech. **528**, 255 (2005).
[50] J. C. Zahnow, J. Maerz, and U. Feudel, Physica D **240**, 882 (2011).
[51] L. Biferale, G. Boffetta, A. Celani, A. Lanotte, and F. Toschi, Phys. Fluids **17**, 021701 (2005).
[52] P. K. Yeung, J. Fluid Mech. **427**, 241 (2001).
[53] P. Vedula, P. K. Yeung, and R. O. Fox, J. Fluid Mech. **433**, 29 (2001).
[54] P. K. Yeung, S. B. Pope, A. G. Lamorgese, and D. A. Donzis, Phys. Fluids **18**, 065103 (2006).